EXAFS Investigations of the Ni Site in *Thiocapsa roseopersicina* Hydrogenase: Evidence for a Novel Ni,Fe,S Cluster

Michael J. Maroney,*,†,‡ Gerard J. Colpas,† Csaba Bagyinka,† Narayan Baidya,§ and Pradip K. Mascharak§

Contribution from the Department of Chemistry and the Program in Molecular and Cellular Biology, University of Massachusetts, Amherst, Massachusetts 01003, and the Department of Chemistry, University of California, Santa Cruz, California 95064. *Received October 19, 1990*

Abstract: The results of the analysis of Ni K-edge EXAFS data from the Ni site in *Thiocapsa roseopersicina* hydrogenase poised in form C are presented. Form C represents a single, reduced, active form of the enzyme. The results obtained from the analysis are consistent with a Ni ligand environment composed of 3 ± 1 N,O donors at 2.06 Å and 2 ± 1 S donors at 2.21 Å. These results are compared with structural data from EXAFS and crystallographic studies of a number of Ni complexes with mixed ligand environments and with the results of EXAFS analyses of the Ni sites of other hydrogenases. The latter comparisons reveal a strong similarity between the data from *T. roseopersicina* and the data from the Fe,Ni,Se enzyme from *Desulfovibrio baculatus*. Data from scattering atoms in the second and third coordination spheres indicate that the Ni center in the enzyme is near to, but not part of, an Fe,S cluster. The data are consistent with Ni-Fe distances of 4.3 and 6.2 Å. Although scattering from S atoms at distances greater than 4 Å makes a negligible contribution to the overall EXAFS spectrum, the fits of Fourier-filtered second coordination sphere EXAFS are improved by the addition of S-scattering atoms at 4.2 Å. These data indicate that Ni-containing hydrogenases contain a novel Fe,S,Ni cluster.

Introduction

Hydrogenases (H_2ases) are metalloenzymes that catalyze the reversible oxidation of H_2 and, as such, are important enzymes in anaerobic metabolism for both chemotrophic and phototrophic bacteria.[1-3] Because they are involved in producing H_2 from water,[4-6] nitrogen fixation,[2,7-12] methane production,[13,14] and sulfate reduction,[3] they have attracted attention as biological catalysts involved in reactions that are of considerable commercial importance.

Hydrogenases contain a complex assembly of metal cofactors and fall into three classes based on their inorganic content.[3] All H_2ases contain Fe,S clusters of various types, and a small group of enzymes containing only Fe and sulfide have been characterized.[15] The vast majority of known H_2ases also contain Ni, and a few enzymes containing Fe, S, Ni, and Se have been characterized.[3] The inorganic content of the H_2ase isolated from the purple photosynthetic bacterium *Thiocapsa roseopersicina* places it in the group containing Fe, S, and Ni.[16] This enzyme has a molecular weight of 98 kDa and is composed of two subunits with molecular weights of 64 and 34 kDa.[17] Analysis of the metal content of the enzyme reveals 7 ± 1 Fe atoms and 1 Ni atom,[16b] placing it among the simplest of the Ni-containing enzymes in terms of metal content.

When Ni is present in the enzyme, it is often detected by an unusual $S = {}^1/_2$ EPR signal that has been assigned to formally Ni(III) or Ni(I) centers.[18] This EPR signal has provided a tool for investigating the role of the Ni center, has provided evidence linking Ni to the binding of H_2 and inhibitors (e.g. CO),[18] and has been used to demonstrate the redox activity of the Ni site. EPR spectra obtained from the Ni site in *Thiocapsa roseopersicina* H_2ase are virtually indistinguishable from those obtained from other Ni-containing H_2ases from both phototrophic and chemotrophic bacteria[19] and indicate that similar Ni sites are employed in all enzymes in this class.

Enzymes in the Fe,Ni class are typically isolated in air as a mixture of both oxidized and inactive forms with distinct EPR spectra.[18] Form A represents a state of the enzyme that has reacted with O_2 and is only slowly reactivated after incubation under H_2. Form B represents a state of the enzyme that is oxidized and inactive but is readily activated upon exposure to H_2. Reduction of either form A or form B proceeds with the formation of an EPR silent state of the Ni center, which is gradually reduced to another EPR active state, form C, that is an active form of the enzyme. EPR spectra obtained at 4 K (where features arising from reduced Fe,S clusters become visible) from H_2ase in form C reveal additional features interpreted as arising from a magnetic interaction between the $S = {}^1/_2$ Ni center and a reduced Fe,S cluster (also $S = {}^1/_2$).[18,19] Further exposure to H_2 produces yet

† Department of Chemistry, University of Massachusetts.
‡ Program in Molecular and Cellular Biology, University of Massachusetts.
§ Department of Chemistry, University of California.

(1) Adams, M. W.; Mortenson, L. E.; Chen, J. S. *Biochim. Biophys. Acta* **1980**, *594*, 105-76.
(2) Vignais, P. M.; Colbeau, A.; Willison, J. C.; Jouanneau, Y. *Adv. Microb. Physiol.* **1985**, *26*, 155-234.
(3) Fauque, G.; Peck, H. D., Jr.; Moura, J. J. G.; Huynh, B. H.; Berlier, Y.; DerVartanian, D. V.; Teixeira, M.; Przybyla, A. E.; Lespinat, P. A.; Moura, I.; LeGall, J. *FEMS Microbiol. Rev.* **1988**, *54*, 299.
(4) Okura, I. *Coord. Rev. Chem. Rev.* **1985**, *68*, 53.
(5) Cuendet, P.; Rao, K. K.; Gratzel, M.; Hall, D. O. *Biochimie* **1986**, *68*, 217-21.
(6) Cammack, R.; Hall, D. O.; Rao, K. K. In *Microbial Gas Metabolism*; Poole, R. K., Dow, C. S., Eds.; Academic Press: Orlando, FL, 1985; Chapter 4.
(7) Bothe, H.; Distler, E.; Eisbrenner, G. *Biochimie*, **1978**, *60*, 277-89.
(8) Chen, Y. P.; Yoch, D. C. *J. Bacteriol.* **1987**, *169*, 4778-83.
(9) Colbeau, A.; Kelley, B. C.; Vignais, P. M. *J. Bacteriol.* **1980**, *144*, 141-8.
(10) Dixon, R. O. *Biochimie* **1978**, *60*, 233-6.
(11) (a) Kondrat'eva, E. N.; Gogotov, I. N.; Gruzinskii, I. V. *Mikrobiologiia* **1979**, *48*, 389-95. (b) Gogotov, I. N. *Biochimie* **1978**, *60*, 267-75.
(12) Mortenson, L. E. *Biochimie* **1978**, *60*, 219-23.
(13) Spencer, R. W.; Daniels, L.; Fulton, G.; Orme-Johnson, W. H. *Biochemistry* **1980**, *19*, 3678-83.
(14) Bastian, N. R.; Wink, D. A.; Wackett, L. P.; Livingston, D. J.; Jordan, L. M.; Fox, J.; Orme-Johnson, W. H.; Walsh, C. T. In *The Bioinorganic Chemistry of Nickel*; Lancaster, J. R., Jr., Ed.; VCH: New York, 1988; Chapter 10.
(15) Adams, M. W. W. *Biochim. Biophys. Acta* **1990**, *1020*, 115.
(16) (a) Kovacs, K. L.; Seefeldt, L. C.; Tigyi, G.; Doyle, C. M.; Mortenson, L. E.; Arp, D. J. *J. Bacteriol.* **1989**, *171*, 430-5. (b) Bagyinka, C.; Szokefalvi-Nagy, Z.; Demeter, I.; Kovacs, K. L. *Biochem. Biophys. Res. Commun.* **1989**, *162*, 422-6.
(17) Kovacs, K.; Tigyi, G.; Thanh, L. T.; Lakatos, S.; Kiss, Z.; Bagyinka, C. *J. Biol. Chem.* **1991**, *266*, 947.
(18) (a) Cammack, R.; Fernandez, V. M.; Schneider, K. In *The Bioinorganic Chemistry of Nickel*; Lancaster, J. R., Ed.; VCH Publishers: New York, 1988; Chapter 8. (b) Moura, J. J. G.; Teixeira, M.; Moura, I.; LeGall, J. *Ibid.*, Chapter 9.
(19) (a) Cammack, R.; Bagyinka, C.; Kovacs, K. L. *Eur. J. Biochem.* **1989**, *182*, 357. (b) Colpas, G. J.; Bagyinka, C.; Maroney, M. J. Unpublished results.

0002-7863/91/1513-3962$02.50/0

another EPR silent form of the protein.[18,19]

EXAFS spectroscopy has been used to probe the ligand environment of the novel redox-active Ni center in "as isolated" samples of H_2ases from chemotrophic bacteria, including *Desulfovibrio gigas*,[20] *Methanobacterium thermoautotrophicum*,[21] and *Desulfovibrio baculatus*.[22] In all cases, evidence for ligation by S-donor ligands has been found, and in the latter case, ligation of the Ni by Se from a selenocysteine residue, as well as S- and O,N-donors, was demonstrated. Herein, we report the results of an EXAFS study of *Thiocapsa roseopersicina* H_2ase poised in form C. Analysis of the spectra obtained from this active form of the enzyme reveals a mixed ligand environment and provides evidence supporting the existence of a novel Fe,S,Ni cluster in the active site.

Experimental Section

Sample Preparation. Structurally characterized model compounds used in this study were synthesized by procedures in the literature as indicated in Table II.

Thiocapsa roseopersicina H_2ase was isolated from bacteria grown on a modified Pfennig's medium under standard photosynthetic conditions. The bacteria were isolated by centrifugation and stored as a cell paste at −20 °C. The enzyme was isolated and purified by using a minor variation of published procedures.[23] Final purification of the H_2ase was achieved by preparative electrophoresis. The enzyme activity was monitored by gas chromatographic quantitation of H_2 production in the presence of reduced methyl viologen.[24] The protein concentration was determined by using the absorbance at 220 nm with bovine serum albumin as a standard. No significant difference in activity was detected in the sample before and after exposure to synchrotron radiation.

The enzyme sample used in the XAS experiments was prepared in 20 mM Tris-HCl buffer (pH 8) that was 20% glycerol and had a Ni concentration of 0.28 mM (vide infra). The concentrated sample was poised in form C using EPR spectroscopy at 77 K to monitor the redox state of the enzyme. The enzyme was first fully reduced by exposure to H_2 overnight (no EPR signal) and was then oxidized back to form C (EPR active) by the addition of a negligible volume of a concentrated anaerobic solution of oxidized benzyl viologen to a final concentration of 2 mM. With use of this method, a sample containing very nearly 100% of the enzyme in form C can be prepared. Integration of the EPR signal from this sample gave a concentration of 0.27 mM spins, or 0.96 spin/protein. The energy of the Ni K-edge was monitored on sequential scans to confirm the stability of the enzyme to reduction, oxidation, or other changes upon exposure to synchrotron radiation. Following data collection, the sample was analyzed for metal content by graphite furnace atomic absorption spectroscopy and was found to have an Fe:Ni ratio of (7 ± 1):1, consistent with published values.[16b]

Data Collection. Ni K-edge X-ray absorption data were collected on beam line X-9A at the National Synchrotron Light Source at Brookhaven National Laboratory. Data were collected under dedicated conditions at ca. 2.53 GeV and 60–120 mA by using a Si(111) double crystal monochromator that was calibrated using the first inflection point of Ni foil (8331.6 eV). This arrangement provided a theoretical resolution of ca. 1 eV at 8.3 keV for a 1 mm hutch slit height, and edge energy calibrations were reproducible to within ±0.2–0.3 eV. Harmonic rejection was accomplished with use of a focusing mirror left flat. Both external and internal edge energy calibration methods were used. Internal calibration was achieved by measuring the small absorbance observed in I_0 due to the Ni mirror used for harmonic rejection.

Model compound data were collected in the transmission mode on powdered samples diluted with boron nitride to reduce thickness effects, using N_2 (I_0) and Ar (I) filled ionization detectors. Spectra were typically run at least twice to check for reproducibility, and the reported spectra may be a single scan or the sum of two scans. Unless otherwise indicated, data were collected at room temperature. Low-temperature data were collected by placing the powdered samples in copper holders that were in thermal contact with liquid N_2 in an evacuated cryostat.

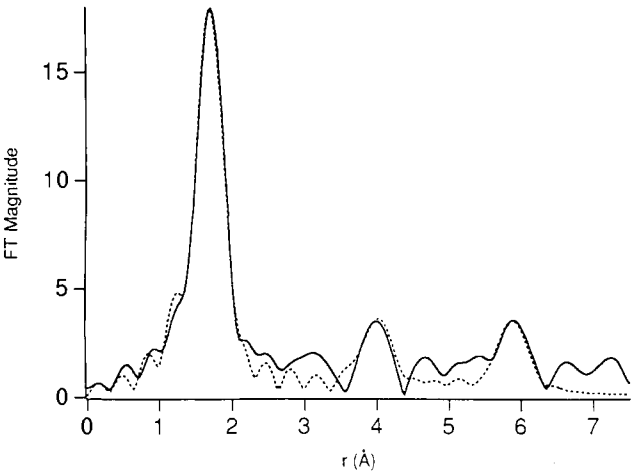

Figure 1. Fourier-transformed Ni K-edge EXAFS spectrum (solid line) from *T. roseopersicina* hydrogenase and a fit (dashed line) generated by using Fourier filtered data with a backtransform window of 1.1–6.5 Å. The fit is from Table III and includes (3) Ni–N = 2.05 Å, (2) Ni–S = 2.21 Å, (2) Ni–Fe = 4.3 Å, (2) Ni–S = 4.2 Å, (2) Ni–Fe = 6.2 Å, and (2) Ni–S = 6.2 Å.

Fluorescence data were collected on a frozen solution of *T. roseopersicina* H_2ase that was ca. 0.3 mM in Ni with use of a 13-element Ge detector (Canberra). The sample was held in thermal contact with liquid N_2 in an evacuated cryostat. The spectra reported are the weighted sums of the data obtained from each element for 20 scans by using the procedure described by Scott.[25]

Data Analysis. The EXAFS data were background corrected and normalized by using standard procedures, which in the case of fluorescence data included corrections for detector efficiencies, absorbance by air and cryostat windows, and the variation with energy of the sample X-ray penetration depth.[26]

Least-squares fits of the enzyme data were performed minimizing the value of R ($R = [\sum k^6(\chi_c - \chi)^2/n]^{1/2}$, where the summation is performed over the n data points in the range of k = 2–12.5) with use of single-scattering EXAFS theory (eqs 1 and 2)[25] and the theoretical amplitude

$$\chi_c = \sum_{\text{shells}}\{NA[f(k)]k^{-1}r^{-2}e^{-2\sigma k^2}\sin(2kr + \alpha(k))\} \quad (1)$$

$$k = [4\pi m_e(E - (8340\text{ eV} + \Delta E))/h]^{1/2} \quad (2)$$

(f) and phase functions (α) of McKale et al. that were obtained from calculations using a full curved wave formalism.[27] The theoretical values were adjusted by using compounds of known structure. Values of A (the amplitude reduction factor), ΔE (the edge energy shift), and σ^2 (Debye–Waller parameter) were obtained for Ni–N(O), Ni–S(P,Cl), and Ni–Ni absorber–scatterer pairs from $[Ni(Im)_6](BF_4)_2$ (r = 2.128 (3) Å, where r is the average Ni–N distance and the error is the standard deviation in the average of the Ni–N distances, A = 0.37, ΔE = 4.5 eV, σ^2 = 0.0044), $(Et_4N)_2[Ni(p\text{-}S\text{-}C_6H_4Cl)_4]$ (r = 2.281 (10) Å, A = 0.46, ΔE = 0.0 eV, σ^2 = 0.0032), and $[Ni(SS_2)]_2$ (data collected at low temperature, r = 2.733 (5) Å, A = 0.51, ΔE = −1.6, eV, σ^2 = 0.0055).[28] In the case of Ni–Fe vectors, the values of A and ΔE used in the fits were obtained from the Ni–Ni interaction in $[Ni(SS_2)]_2$ and used with the theoretical phase shift for Fe.

The values of A, ΔE, and σ^2 obtained from these models were used in the refinement of EXAFS data from the enzyme and other model compounds with the restricted fit protocol.[26] In this fitting strategy, only r (the absorber–scatterer distance) and σ^2 are refined for a particular shell, with the value of N (number of identical scatterers) restrained to

(20) (a) Scott, R. A.; Wallin, S. A.; Czechowski, M.; DerVartanian, D. V.; LeGall, J.; Peck, H. D., Jr.; Moura, I. *J. Am. Chem. Soc.* **1984**, *106*, 6864. (b) Scott, R. A.; Czechowski, M.; DerVartanian, D. V.; LeGall, J.; Peck, H. D., Jr.; Moura, I. *Rev. Port. Quim.* **1985**, *27*, 67.

(21) Lindahl, P. A.; Kojima, N.; Hausinger, R. P.; Fox, J. A.; Teo, B. K.; Walsh, C. T.; Orme-Johnson, W. H. *J. Am. Chem. Soc.* **1984**, *106*, 3062.

(22) Eidsness, M. K.; Scott, R. A.; Prickril, B. C.; DerVartanian, D. V.; LeGall, J.; Moura, I.; Moura, J. J. G.; Peck, H. D., Jr. *Proc. Natl. Acad. Sci. U.S.A.* **1989**, *86*, 147.

(23) Kovacs, K. L.; Tigyi, G.; Alfonz, H. *Prep. Biochem.* **1985**, *15*, 321.

(24) Bagyinka, C.; Zorin, N. A.; Kovacs, K. L. *Anal. Biochem.* **1984**, *142*, 7.

(25) Scott, R. A. *Meth. Enzymol.* **1985**, *117*, 414.

(26) Scarrow, R. C.; Maroney, M. J.; Palmer, S. M.; Que, L., Jr.; Roe, A. L. *J. Am. Chem. Soc.* **1987**, *109*, 7857.

(27) McKale, A. G.; Veal, B. W.; Paulikas, A. P.; Chan, S.-K.; Knapp, G. S. *J. Am. Chem. Soc.* **1988**, *110*, 3763.

(28) Abbreviations used: bimp, 2,6-bis[(bis((1-methylimidazol-2-yl)-methyl)amino)methyl]-4-methylphenolate; bpy, 2,2′-bipyridine; edt, 1,2-ethanedithiolate; Im, imidazole; Me_6tren, tris(2-(dimethylamino)ethyl)amine; MPG, *N*-(2-mercaptopropionyl)glycinate; mnt, *cis*-1,2-dicyanoethylene-1,2-dithiolate; NS_2SMe, bis(2-mercaptoethyl)(2-methylthioethyl)amine; N_2S_2, *N,N′*-dimethyl-*N,N′*-bis(2-mercaptoethyl)-1,3-propanediamine; OAc, acetate; pdtc, pyridine-2,6-bis(monothiocarboxylate); pm2S, pyrimidine-2-thiolate, p_3, tris(2-(diphenylphosphino)ethyl)methane; pp_3, tris(2-(diphenylphosphino)-ethyl)phosphine; py2S, pyridine-2-thiolate; SS_2, bis(2-mercaptoethyl) sulfide; tren, tris(2-aminoethyl)amine; ttcn, 1,4,7-trithiocyclononane.

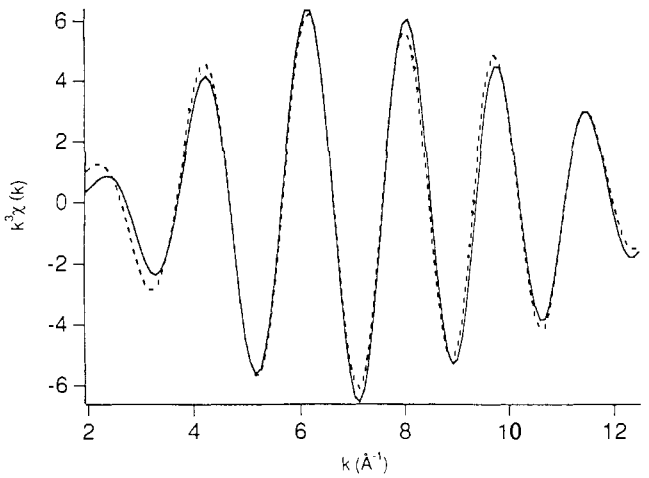

Figure 2. Fourier-filtered Ni K-edge EXAFS spectrum from atoms in the first coordination sphere (backtransform window = 1.1–2.3 Å) of Ni in *T. roseopersicina* hydrogenase (solid line). The fit shown (dashed line) is from Table I and includes (3) Ni–N 2.06 Å and (2) Ni–S 2.21 Å.

fixed integer values. The quality of the fits generated is judged by minimum values of R and $\Delta\sigma^2 = \sigma^2(\text{fit}) - \sigma^2(\text{model})$.

To isolate contributions from specific coordination spheres and minimize the number of adjustable parameters, fits involving Fourier filtering of both χ_c and χ were employed. For first coordination sphere scatterers, a backtransform window of 1.1–2.3 Å was employed. The backtransform windows used for second and third coordination sphere scattering atoms are noted in the text. The results from fits of Fourier-filtered data were subsequently re-examined by generating multishell fits to the unfiltered data, which also allowed the cubic spline parameters for the background correction to be independently refined.

Weak features arising from atoms in the second and third coordination sphere of Ni were examined carefully by using subsets of the data and different truncation limits in the Fourier transform. The peaks reported were in all subsets of the data and did not change position when the data were truncated between 10 and 12.5 Å^{-1}, although a loss of resolution (the peaks are broader) is noted in the shorter data sets.

Results and Discussion

First Coordination Sphere. The Fourier-transformed EXAFS spectrum (not corrected for phase shifts) from the Ni site in *Thiocapsa roseopersicina* H_2ase is shown in Figure 1. The data reveal peaks arising from scattering atoms in the first, second, and third coordination spheres of the Ni atom. The results of fits generated to Fourier-filtered first coordination sphere (r = 1.1–2.3 Å) EXAFS data are summarized in Table I and Figure 2. Table I contains all possible fits using any combination of N- and S-scatterers for coordination numbers 4–6. The best fit is calculated for a five-coordinate Ni site containing three N,O-scattering atoms at 2.06 (2) Å and two S-scattering atoms at 2.21 (2) Å.[29] Data obtained from the analysis of edge features substantiate the coordination number, are consistent with a mixed ligand environment, and are most consistent with a distorted trigonal-bipyramidal geometry.[30]

From examination of Table I, it is clear that only fits involving a mixed-donor coordination environment with these Ni–ligand bond distances model the experimental data. However, fits that are nearly as good as the best fit can be obtained for four-, five-, or six-coordinate sites with 1–3 S-donor ligands. The exact mix of ligands and the overall coordination number of the Ni are not determined with a high degree of confidence from the EXAFS data analysis alone. This situation arises because the number of identical scattering atoms (N) is a poorly determined parameter that is highly correlated with σ^2 and dependent on the value of the empirically determined amplitude reduction factor (A).[25] A model study was undertaken in order to test the reliability of the distances and coordination environment determined for the H_2ase

Table I. Fits of First Coordination Sphere[a] Fourier-Filtered Ni EXAFS from Hydrogenase

CN[b]	N[c]	r,[d] Å	$10^3\Delta\sigma^2$,[e] Å^2	correl coeff > 0.6	R[f]
6	6	Ni–S = 2.217 (3)	4.8 (5)		1.69
	5	Ni–S = 2.226 (3)	8.0 (5)		0.79
	1	Ni–N = 2.059 (2)	−12.0 (2)		
	4	Ni–S = 2.218 (3)	7.9 (4)		0.55
	2	Ni–N = 2.062 (2)	−9.0 (2)		
	3	Ni–S = 2.206 (3)	6.5 (4)	r_S/r_N = −0.67;	0.41
	3	Ni–N = 2.065 (1)	−7.1 (2)	σ^2_S/σ^2_N = −0.71	
	2	Ni–S = 2.192 (3)	2.9 (5)	r_S/r_N = −0.77;	0.40
	4	Ni–N = 2.068 (2)	−5.2 (3)	σ^2_S/σ^2_N = −0.88	
	1	Ni–S = 2.201 (4)	−3.1 (4)	r_S/r_N = −0.82;	0.57
	5	Ni–N = 2.056 (3)	−2.7 (4)	σ^2_S/σ^2_N = −0.85	
	6	Ni–N = 2.058 (2)	−4.9 (2)		1.11
5	5	Ni–S = 2.214 (3)	3.0 (4)		1.51
	4	Ni–S = 2.226 (3)	5.1 (4)		0.67
	1	Ni–N = 2.055 (2)	−11.7 (2)		
	3	Ni–S = 2.200 (2)	4.2 (3)	r_S/r_N = −0.64	0.44
	2	Ni–N = 2.057 (2)	−8.6 (2)		
	2	Ni–S = 2.213 (2)	1.6 (4)	r_S/r_N = −0.77;	0.34
	3	Ni–N = 2.057 (2)	−6.4 (2)	σ^2_S/σ^2_N = −0.72	
	1	Ni–S = 2.222 (4)	−3.3 (3)	r_S/r_N = −0.69;	0.44
	4	Ni–N = 2.044 (2)	−4.5 (2)	r_S/σ^2_N = −0.71; r_N/σ^2_S = 0.74	
	5	Ni–N = 2.058 (2)	−5.9 (2)		1.08
4	4	Ni–S = 2.210 (3)	1.1 (3)		1.36
	3	Ni–S = 2.226 (2)	2.9 (3)	r_N/σ^2_S = −0.72	0.60
	1	Ni–N = 2.046 (3)	−11.3 (2)		
	2	Ni–S = 2.227 (2)	−0.3 (3)	r_S/σ^2_N = 0.81	0.41
	2	Ni–N = 2.043 (2)	−8.3 (2)		
	1	Ni–S = 2.237 (2)	−4.9 (3)	r_S/σ^2_N = −0.86;	0.40
	3	Ni–N = 2.033 (2)	−7.3 (2)	r_N/σ^2_S = −0.86	
	4	Ni–N = 2.059 (2)	−7.1 (2)		1.17

[a] Backtransform window = 1.1–2.3 Å. [b] Coordination number. [c] Number of identical scattering atoms used in the fit. [d] Bond lengths of atoms in the first coordination sphere in compounds of known structure are generally reproduced within 0.02 Å. [e] $\Delta\sigma^2 = \sigma^2(\text{fit}) - \sigma^2(\text{model})$. [f] $R = [\sum k^6(\chi_c - \chi)^2/n]^{1/2}$.

Ni site from our EXAFS analysis and to test the transferability of semiempirical parameters obtained from homoleptic and high-symmetry Ni(II) models to low-symmetry cases involving mixed ligand environments and/or different formal oxidation states for Ni. This study consists of the analysis of 18 model compounds chosen to emphasize mixed ligand environments and includes two examples of isoleptic pairs of Ni complexes in the II and III oxidation states. The Ni–S bond lengths involved range from 2.18 Å in several planar four-coordinate complexes to 2.53 Å in a highly disordered six-coordinate complex. The range of Ni–O,N bond lengths was from 1.88 to 2.15 Å. The results of this study, which was performed by using data limits and procedures identical with those used in the analysis of the enzyme data, are summarized in Table II. Only the best fit(s) (based on minimum values of R and $\Delta\sigma^2$, shown in bold face type) and any other fit that is close to the quality of the best fit (as judged by an R value within 0.1 of the R value of the best fit and values of $\Delta\sigma^2 < \pm 10^{-2}$) are shown in Table II. In two four-coordinate cases, $Ni(mnt)_2^{2-}$ and $[Ni_3(MPG)_3]^{3-}$, the fits selected by these criteria do not include a fit of the correct coordination number. Since this information can often be obtained from edge data, the best fits of the correct coordination number are also included in these cases. A table similar to Table I containing all possible fits for coordination numbers 4–6 for each of the model compounds is included as supplementary material.

A comparison of the bond lengths found from EXAFS analysis and the average values of corresponding bond lengths from

(29) Maroney, M. J.; Colpas, G. J.; Bagyinka, C. *J. Am. Chem. Soc.* **1990**, *112*, 7067.

(30) Colpas, G. J.; Maroney, M. J.; Bagyinka, C.; Kumar, M.; Willis, W. S.; Suib, S. L.; Baidya, N.; Mascharak, P. K. *Inorg. Chem.* **1991**, *30*, 920.

crystallographic studies (Table II) confirms the reliability of the EXAFS analysis employed for both Ni(II) and Ni(III) complexes. For Ni–S(Cl) bonds, the differences between the EXAFS distances from the best fits and the crystallographic distances range from −0.04 to 0.00 Å, with an average of −0.02 Å. Modeling P-donor ligands as S-donors is seen to lead to larger errors in r. Excluding the Ni–N distances determined for $Ni(N_2S_2)$, the range of differences between the EXAFS and crystallographic distances range from +0.02 to −0.05 Å, with an average of 0.00. These errors in bond lengths determined by EXAFS are of similar magnitude to the standard deviation in the average of the crystallographic bond lengths. In the case of $Ni(N_2S_2)$, a number of large correlations exist (Table II) and it is clear that the two shells are not refined independently. The effect of these correlations is a large error in the Ni–N bond length (0.2 Å). It is noteworthy that the fit obtained for the correct mix of S- and N-donor ligands does not suffer from these correlations and predicts an accurate value of the Ni–N distance, although the value of $\Delta\sigma^2$ is unacceptably large. One indication of a dubious bond length determination appears to be large differences in the distances determined as a function of coordination number and mix of ligand donor atoms. This is clearly not the case for the analysis of the H_2ase EXAFS data (Table I).

As anticipated, it was more difficult to predict the number of S- and N-donor ligands from the EXAFS data. Excluding the complexes with P-donor ligands, the correct ligand environment was predicted by the best EXAFS fit five times (of which four of the complexes contained only a single type of scattering atom), although the correct ligand environment was among the fits chosen by the selection criteria in 13 cases. In these 13 cases, the best fit never differed by more than one atom of each type from the correct ligand environment. In two planar four-coordinate cases, $Ni(mnt)_2^{2-}$ and $[Ni_3(MPG)_3]^{3-}$, the correct ligand environment was not predicted by the EXAFS data. In the case of the mnt complex, the best fit contains one extra N-donor and one extra S-donor ligand. In the case of the highly distorted trinuclear complex, where each Ni atom exists in a distinct NOS_2 environment,[42] the best fit of the correct coordination number does predict the correct mix of ligands, although the value of R is unacceptably large and the fit features parameters that are moderately correlated. In the case of the dimeric $[Ni(NS_2SMe)]_2$ complex, the single N-donor to each Ni is not observable in the room temperature data and is poorly determined even at low temperature. Two factors appear to be involved. First, the EXAFS is dominated by the presence of three S-donor ligands at short distances. In fact, room temperature data are fit best by three S-donors (Table IV). Second, the dimeric compound has two similar but distinct Ni sites with the largest differences involving the N-donor atom.[31] Thus, static as well as dynamic disorder contributes to the Debye–Waller parameter for this scattering atom.

The Ni–S distance found in Ni thiolates is sensitive to the number of d electrons in the Ni 3d orbital used to form the σ-bond with the thiolate. Terminal Ni–S distances in planar thiolates (all diamagnetic) are the shortest, ranging from 2.14 Å in Ni(tsalen)[43] and $[Ni(MSA)SPh]^-$[44] to 2.22 Å in the planar dimeric complexes $[Ni_2(SPh)_6]^{2-}$[31] and $[Ni_2(SEt)_6]^{2-}$.[45] Five-coordinate complexes in either pyramidal or trigonal-bipyramidal geometries may be either high spin ($S = 1$) or low spin ($S = 0$),[46] and feature Ni–S bond lengths in the 2.2–2.3-Å range. No structurally characterized examples of pyramidal Ni complexes with terminal thiolate ligands exist. One recently reported example of a dinuclear high-spin complex with this geometry ({Ni[*N*-[2-(2-pyridyl)ethyl]-*N*-[2-(methylthio)ethyl]-2-aminoethanethiolate]}$_2$) features Ni–S bond lengths of ca. 2.20 and 2.25 Å for asymmetric bridging thiolates in the basal planes of the Ni centers.[47] For trigonal-bipyramidal geometry, two Ni thiolate complexes have been characterized. The distances found are 2.26 Å for the axial thiolate in low-spin $[Ni(pp_3)SH]^+$[36a] and 2.27 and 2.33 Å for the equatorial thiolates in high-spin [Ni(terpy)(S-2,4,6-(i-Pr)$_3$C$_6$H$_2$)$_2$].[48] The longest Ni–S bond lengths are observed in six-coordinate (all $S = 1$) Ni(II) thiolate complexes, which occur in the ca. 2.4–2.5 Å range (Table II), including the recently reported complex $[Ni(terpy)(C_6F_5S)_2(CH_3CN)]$ (av Ni–S = 2.49 Å).[48]

The Ni–S distance observed in H_2ase form C (2.21 Å) is far too short for a six-coordinate Ni(II) complex. If the EPR activity associated to this site is ascribed to a metal-centered redox process, then the center must be assigned to a formal oxidation state of either I or III. Because form C represents a reduced form of the enzyme, the I formalism is most appropriate and would be expected to give rise to a *lengthening* of the Ni–S bonds. The Ni–S distance would be expected to shorten if form C were a Ni(III) complex, although the only structurally characterized Ni(III) complex with S-donor ligands (albeit not thiolates) features a shortening of the Ni–S bonds by ca. 0.14 Å (see $Ni(pdtc)_2^{2-,-}$, Table II). This degree of bond shortening would not be expected to cause most Ni–S distances in six-coordinate complexes to lie near the distance found in the enzyme. Distances characteristic of Ni–thiolate bonds in known distorted tetrahedral (all $S = 1$) structures (e.g. $[Ni(S\text{-}p\text{-}C_6H_4Cl)_4]^{2-}$,[49] av Ni–S = 2.28 Å; $[Ni(SPh)_4]^{2-}$,[50] av Ni–S = 2.29 Å) are shorter than in $S = 1$ six-coordinate complexes, but comparable with the Ni(III) structure mentioned above. Given the range of Ni–S distances and their dependency on geometry and spin state, a six-coordinate structure for the Ni site in form C may be ruled out.

The Ni–O,N distance found in the enzyme could be accomplished by a Ni site of any coordination number (see Table II for examples), although most Ni–N distances in planar complexes are shorter than 2.06 Å and Ni–O bonds are in general shorter than Ni–N bonds. The Ni–N,O distance found in the enzyme is identical with the average Ni–N distances found in the trigonal-bipyramidal $[Ni(Me_6tren)NCS]NCS$ and [Ni(terpy)(S-2,4,6-(i-Pr)$_3$C$_6$H$_2$)$_2$] complexes and is also appropriate for six-coordinate complexes.

Taken together, the Ni–S and Ni–O,N bond lengths determined for the Ni site in the enzyme are most consistent with a five-

(31) Colpas, G. J.; Kumar, M.; Day, R. O.; Maroney, M. J. *Inorg. Chem.* **1990**, *29*, 4779–88.
(32) (a) Osakada, K.; Yamamoto, T.; Yamamoto, A.; Takenaka, A.; Sasada, Y. *Acta Crystallogr.* **1984**, *C40*, 85. (b) Yamamoto, T.; Sekine, Y. *Inorg. Chem. Acta* **1984**, *83*, 47.
(33) Rosenfield, S. G.; Berends, H. P.; Gelmini, L.; Stephan, D. W.; Mascharak, P. K. *Inorg. Chem.* **1987**, *26*, 2792.
(34) Krüger, H.-J.; Holm, R. H. *J. Am. Chem. Soc.* **1990**, *112*, 2955.
(35) Setzer, W. N.; Ogle, C. A.; Wilson, G. S.; Glass, R. S. *Inorg. Chem.* **1983**, *22*, 266.
(36) (a) Bertini, I.; Ciampolini, M.; Dapporto, P.; Gatieshi, D. *Inorg. Chem.* **1972**, *11*, 2254. (b) Ciampolini, M.; Nardi, N. *Inorg. Chem.* **1966**, *5*, 41.
(37) Di Vaira, M.; Midollini, S.; Sacconi, L. *Inorg. Chem.* **1977**, *16*, 1518.
(38) Ghilardi, C. A.; Midollini, S.; Sacconi, L. *Inorg. Chem.* **1975**, *14*, 1790.
(39) (a) Baidya, N.; Stephan, D. W.; Campagna, C. S.; Mascharak, P. K. *Inorg. Chim. Acta* **1990**, *177*, 233. (b) Structure of Ph_3MeP^+ salt: Yamamura, T.; Kurihara, H.; Nakamura, N.; Kuroda, R.; Asakura, K. *Chem. Lett.* **1990**, 101.
(40) (a) Kobayashi, A.; Sasaki, Y. *Bull. Chem. Soc. Jpn.* **1977**, *50*, 2650. (b) Gray, H. B.; Williams, R.; Bernal, I.; Billig, E. *J. Am. Chem. Soc.* **1962**, *84*, 3596. (c) Davison, A.; Edelstein, N.; Holm, R. H.; Maki, A. H. *J. Am. Chem. Soc.* **1963**, *85*, 2029.
(41) (a) Barclay, G. A.; McPartlin, E. M.; Stephenson, N. C. *Acta Crystallogr.* **1969**, *B25*, 1262. (b) Baker, D. J.; Goodall, D. C.; Moss, D. S. *Chem. Commun.* **1969**, 325.
(42) Baidya, N.; Olmstead, M. M.; Mascharak, P. M. *Inorg. Chem.* **1989**, *28*, 3426.
(43) Yamamura, T.; Tadokoro, M.; Kuroda, R. *Chem. Lett.* **1989**, 246.
(44) Kanatzidis, M. G. *Inorg. Chim. Acta* **1990**, *168*, 101.
(45) Watson, A. D.; Rao, Ch. P.; Dorfman, J. R.; Holm, R. H. *Inorg. Chem.* **1985**, *24*, 2820.
(46) Sacconi, T. *Trans. Met. Chem.* **1968**, *4*, 199.
(47) Handa, M.; Mikuriya, M.; Okawa, H.; Kida, S. *Chem. Lett.* **1988**, 1555.
(48) Baidya, N.; Olmstead, M.; Mascharak, P. K. *Inorg. Chem.* **1991**, *30*, 929.
(49) Rosenfield, S. G.; Armstrong, W. H.; Mascharak, P. M. *Inorg. Chem.* **1986**, *25*, 3014.
(50) (a) Holah, D. G.; Coucouvanis, D. *J. Am. Chem. Soc.* **1975**, *97*, 6917. (b) Swenson, D.; Baenziger, N. C.; Coucouvanis, D. *J. Am. Chem. Soc.* **1978**, *100*, 1932.

Table II. Fits of First Coordination Sphere[a] Fourier-Filtered EXAFS Data from Structurally Characterized Models[b]

sample	CN	*N*	*r*, Å	$10^3\Delta\sigma^2$, Å^2	correl coeff > 0.6	*R*	av crystallographic bond lengths (σ),[c] Å	ref
$[Ni(tren)_2](BF_4)_2$	**6**	**6**	**Ni–N = 2.145 (1)**	**−0.1 (2)**		**0.30**	(6) Ni–N = 2.149 (22)	31
	5	5	Ni–N = 2.145 (2)	−1.6 (2)		0.39		
$[Ni(bpy)_2(SPh)_2]$	6	3	Ni–S = 2.396 (2)	7.7 (3)		0.23	(2) Ni–S = 2.445 (2)	32
		3	Ni–N = 2.080 (1)	−2.4 (2)			(4) Ni–N = 2.091 (9)	
		2	**Ni–S = 2.407 (1)**	**4.1 (2)**		**0.20**		
		4	**Ni–N = 2.088 (1)**	**−0.9 (2)**				
		1	**Ni–S = 2.417 (2)**	**−1.0 (2)**		**0.24**		
		5	**Ni–N = 2.099 (1)**	**0.2 (2)**				
$Et_4N[Ni(py2S)_3]$	6	3	Ni–S = 2.483 (2)	7.1 (3)		0.31	(3) Ni–S = 2.528 (12)	33
		3	Ni–N = 2.050 (1)	−3.4 (2)			(3) Ni–N = 2.052 (25)	
		2	**Ni–S = 2.487 (1)**	**1.9 (2)**		**0.21**		
		4	**Ni–N = 2.053 (1)**	**−0.4 (2)**				
		1	Ni–S = 2.487 (2)	−3.7 (2)		0.30		
		5	Ni–N = 2.060 (2)	4.0 (3)				
	5	2	Ni–S = 2.483 (1)	2.7 (2)		0.20		
		3	Ni–N = 2.053 (1)	−2.8 (1)				
		1	Ni–S = 2.485 (1)	−3.3 (1)		0.21		
		4	Ni–N = 2.058 (1)	1.1 (2)				
	4	1	Ni–S = 2.483 (2)	−2.8 (2)		0.27		
		3	Ni–N = 2.056 (2)	−1.6 (2)				
$Et_4N[Ni(pm2S)_3]$	6	3	Ni–S = 2.454 (2)	4.3 (3)		0.39	(3) Ni–S = 2.495 (44)	33
		3	Ni–N = 2.052 (2)	−3.1 (2)			(3) Ni–N = 2.043 (16)	
		2	**Ni–S = 2.461 (1)**	**0.1 (2)**		**0.29**		
		4	**Ni–N = 2.059 (2)**	**0.1 (2)**				
		1	Ni–S = 2.465 (1)	−4.8 (1)		0.32		
		5	Ni–N = 2.070 (2)	4.6 (4)				
	5	2	Ni–S = 2.457 (2)	0.6 (2)		0.36		
		3	Ni–N = 2.059 (2)	−2.4 (3)				
		1	Ni–S = 2.463 (2)	−4.6 (2)		0.37		
		4	Ni–N = 2.069 (3)	1.9 (4)				
$(Et_4N)_2[Ni(pdtc)_2]$	6	4	Ni–S = 2.387 (7)	3.2 (1)		0.22	(4) Ni–S = 2.418 (15)	34
		2	Ni–N = 2.032 (2)	−3.9 (2)			(2) Ni–N = 2.047 (2)	
		3	**Ni–S = 2.393 (1)**	**0.6 (1)**		**0.20**		
		3	**Ni–N = 2.049 (1)**	**−1.0 (2)**				
$Bz(Ph)_3P[Ni(pdtc)_2]$	6	**5**	**Ni–S = 2.254 (1)**	**1.8 (1)**		**0.28**	(4) Ni–S = 2.279 (11)	34
		1	**Ni–N = 1.985 (5)**	**−2.1 (7)**			(2) Ni–N = 2.037 (5)	
		4	Ni–S = 2.258 (1)	0.3 (1)		0.33		
		2	Ni–N = 1.999 (3)	−1.7 (5)				
	5	4	Ni–S = 2.256 (1)	−0.3 (1)	$\sigma^2_S/\sigma^2_N = 0.71$	0.27		
		1	Ni–N = 1.990 (2)	−7.3 (3)				
$[Ni(ttcn)_2](BF_4)_2$	6	**6**	**Ni–S = 2.384 (1)**	**2.7 (1)**		**0.40**	(6) Ni–S = 2.386 (13)	35
	5	**5**	**Ni–S = 2.383 (1)**	**1.3 (1)**		**0.46**		
$[Ni(Me_6tren)NCS]NCS$	6	**6**	**Ni–N = 2.079 (2)**	**3.2 (3)**		**0.34**	(5) Ni–N = 2.06 (6)	36
	5	**5**	**Ni–N = 2.079 (2)**	**1.2 (3)**		**0.38**		
$[Ni(Me_6tren)Cl]Cl$	6	**1**	**Ni–S = 2.284 (2)**	**−2.0 (2)**		**0.28**	(1) Ni–Cl = 2.295 (2)[d]	31
		5	**Ni–N = 2.102 (2)**	**3.5 (4)**			(4) Ni–N = 2.123 (36)[d]	
		2	Ni–S = 2.272 (4)	2.8 (6)	$\sigma^2_N/\sigma^2_S = -0.87$; $r_N/r_S = -0.77$	0.42		
		4	Ni–N = 2.131 (5)	3 (1)				
	5	1	Ni–S = 2.296 (3)	7.7 (3)	$r_S/\sigma^2_N = -0.72$	0.34		
		4	Ni–N = 2.095 (3)	0.2 (4)				
$[Ni(pp_3)SH]BPh_4$	6	**5**	**Ni–S = 2.190 (2)**	**3.4 (1)**		**0.54**	(5) Ni–S(P) = 2.249 (50)	37
		1	**Ni–N = 1.786 (10)**	**0.1 (1)**				
	5	4	Ni–S = 2.191 (1)	1.6 (2)		0.60		
		1	Ni–N = 1.826 (11)	0.1 (2)				
$[Ni(pp_3)H]BF_4$	5	5	Ni–S = 2.186 (3)	5.3 (3)		1.00	Ni(II) analog of structurally characterized Co(I) complex	38
	4	**4**	**Ni–S = 2.184 (2)**	**3.1 (2)**		**0.74**		

Table II (Continued)

sample	CN	*N*	*r*, Å	$10^3\Delta\sigma^2$, Å^2	correl coeff > 0.6	*R*	av crystallographic bond lengths (σ),[c] Å	ref
$(PPh_4)_2[Ni(edt)_2]$	6	4	Ni-S = 2.179 (1)	−0.1 (1)		0.27	(4) Ni-S = 2.195 (9)	39
		2	Ni-N = 1.286 (7)	0.2 (5)				
	4	**4**	**Ni-S = 2.179 (1)**	**0.0 (1)**		**0.24**		
		3	Ni-S = 2.185 (1)	−2.3 (1)	$\sigma^2_S/\sigma^2_N = 0.72$	0.31		
		1	Ni-N = 1.926 (3)	−5.7 (4)				
$(Et_4N)_2[Ni(mnt)_2]$	6	**5**	**Ni-S = 2.176 (1)**	**−1.2 (1)**		**0.62**	(4) Ni-S = 2.175 (2)	40
		1	**Ni-N = 1.867 (5)**	**−6.9 (5)**				
	5	4	Ni-S = 2.178 (1)	−2.8 (1)	$r_S/r_N = 0.60$; $\sigma^2_S/\sigma^2_N = 0.69$	0.60		
		1	Ni-N = 1.892 (4)	−8.6 (4)				
	4	3	Ni-S = 2.180 (1)	−4.9 (1)	$r_S/r_N = 0.73$; $\sigma^2_S/\sigma^2_N = 0.81$	0.88		
		1	Ni-N = 1.912 (4)	−10.8 (5)				
$Et_4N[Ni(mnt)_2]$	5	**4**	**Ni-S = 2.144 (1)**	**−1.2 (1)**		**0.66**	(4) Ni-S = 2.149 (3)	40
		1	**Ni-N = 1.756 (15)**	**2 (2)**				
	4	4	Ni-S = 2.144 (1)	−1.2 (1)		0.74		
$[Ni(SS_2)]_2$ (77 K)	5	4	Ni-S = 2.170 (1)	−0.5 (1)		0.70	(4) Ni-S = 2.18 (3)	41
		1	Ni-N = 1.728 (21)	6 (3)				
	4	4	Ni-S = 2.169 (1)	−0.4 (1)		0.74		
		2	**Ni-S = 2.174 (1)**	**−4.7 (1)**		**0.69**		
		2	**Ni-N = 1.919 (8)**	**0 (1)**				
$[Ni(NS_2SMe)]_2$	**4**	**4**	**Ni-S = 2.164 (1)**	**3.3 (2)**		**0.55**	(3) Ni-S = 2.184 (25) (1) Ni-N = 1.953 (11)	31
		1	Ni-S = 2.170 (2)	−5.0 (2)	$r_S/\sigma^2_N = -0.65$	0.65		
		3	Ni-N = 1.946 (6)	2 (1)				
$[Ni(NS_2SMe)]_2$ (77 K)	5	2	Ni-S = 2.169 (1)	−3.7 (1)		0.37		
		3	Ni-N = 1.906 (5)	9 (1)				
	4	3	Ni-S = 2.167 (1)	−1.6 (1)		0.40		
		1	Ni-N = 1.846 (7)	−0.7 (1)				
		2	**Ni-S = 2.170 (1)**	**−4.0 (1)**		**0.28**		
		2	**Ni-N = 1.905 (3)**	**1.5 (1)**				
$[Ni(N_2S_2)]$	6	4	Ni-S = 2.179 (1)	1.8 (2)	$r_N/\sigma^2_S = 0.88$; $r_S/\sigma^2_N = -0.83$; $r_S/r_N = 0.64$	0.32	(2) Ni-S = 2.175 (1) (2) Ni-N = 2.003 (5)	31
		2	Ni-N = 2.295 (6)	−4.8 (5)				
	5	**3**	**Ni-S = 2.163 (1)**	**−0.2 (1)**	$r_S/r_N = 0.62$; $\sigma^2_S/\sigma^2_N = 0.73$	**0.23**		
		2	**Ni-N = 2.193 (8)**	**9 (2)**				
	4	**3**	**Ni-S = 2.163 (2)**	**−0.5 (4)**	$r_S/r_N = 0.95$; $\sigma^2_S/\sigma^2_N = 0.98$	**0.31**		
		1	**Ni-N = 2.201 (19)**	**−2 (2)**				
		2	Ni-S = 2.162 (1)	−2.1 (1)		0.30		
		2	Ni-N = 2.016 (9)	13 (2)				
$(NH_4)_3[Ni_3(MPG)_3]$	6	**4**	**Ni-S = 2.167 (1)**	**−1.0 (1)**		**0.49**	(2) Ni-S = 2.184 (23) (2) Ni-O,N = 1.876 (32)	42
		2	**Ni-N = 1.869 (1)**	**−9.4 (1)**				
		3	**Ni-S = 2.175 (1)**	**−3.1 (1)**		**0.50**		
		3	**Ni-N = 1.881 (1)**	**−7.8 (1)**				
	4	2	Ni-S = 2.173 (2)	−5.8 (2)	$r_S/r_N = 0.68$; $\sigma^2_S/\sigma^2_N = 0.78$	1.15		
		2	Ni-N = 1.889 (3)	−10.6 (3)				

[a] Backtransform window = 1.1–2.3 Å. [b] Parameters are defined in Table I. [c] Numbers in parentheses indicate the standard deviation in the average of the crystallographic bond lengths in the first coordination sphere. [d] From the crystal structure of the salt formed with $[Ni_2(S\text{-}p\text{-}C_6H_4Cl)_6]^{2-}$.

coordinate structure. Such a structure is also consistent with EPR data from the enzyme.[18,19] Employing the standard crystal field analysis of the EPR spectrum, the *g* values ($g_z < g_x, g_y$) indicate that the spin density on Ni resides in a d_{z^2} orbital. This is the expected electronic structure for a trigonal-bipyramidal Ni(I) complex.[51]

In the case of H_2ase form C, additional uncertainty about the Ni coordination environment arises from the possibility that a hydride ligand might exist in the Ni coordination sphere.[52] A hydride ligand would not be expected to contribute to the observed EXAFS experiment, a fact that is confirmed at least in part by the data from the model compound $[Ni(pp_3)H]BF_4$ (Table II), which is best modeled as a NiS_4 case (and will not refine an N-donor ligand). Thus, the existence of a possible hydride ligand in form C cannot be addressed from EXAFS data, and a site consisting of four or five endogenous ligands and a hydride cannot be entirely ruled out.

Although the Ni–S distances obtained for the Ni site in *T. roseopersicina* H_2ase are similar to those obtained in other H_2ases from EXAFS analysis, the study presented here provides the first evidence of ligands involving low Z donor atoms in this class of enzyme. Given the similarity of the EPR spectra, it seems unlikely that substantially different sites are present in the Fe,Ni enzymes from chemotrophs and phototrophs.[18] Two possible reasons for the differing analyses are plausible. First, the analysis presented here uses curved wave parameters that allow the data to be fit to $k = 2.0$, and data at smaller values of *k* emphasize scattering

(51) Salerno, J. C. In *The Bioinorganic Chemistry of Nickel*; Lancaster, J. R., Jr., Ed.; VCH: New York, 1988; Chapter 3.

(52) (a) van der Zwaan, J. W.; Albracht, S. P. J.; Fontijn, R. D.; Mul, P. *Eur. J. Biochem.* **1987**, *169*, 377. (b) Teixeira, M.; Moura, I.; Xavier, A. V.; Huynh, B. H.; DerVartanian, D. V.; Peck, H. D., Jr.; LeGall, J.; Moura, J. J. G. *J. Biol. Chem.* **1985**, *260*, 8942. (c) Crabtree, R. H. *Inorg. Chim. Acta* **1986**, *125*, L7.

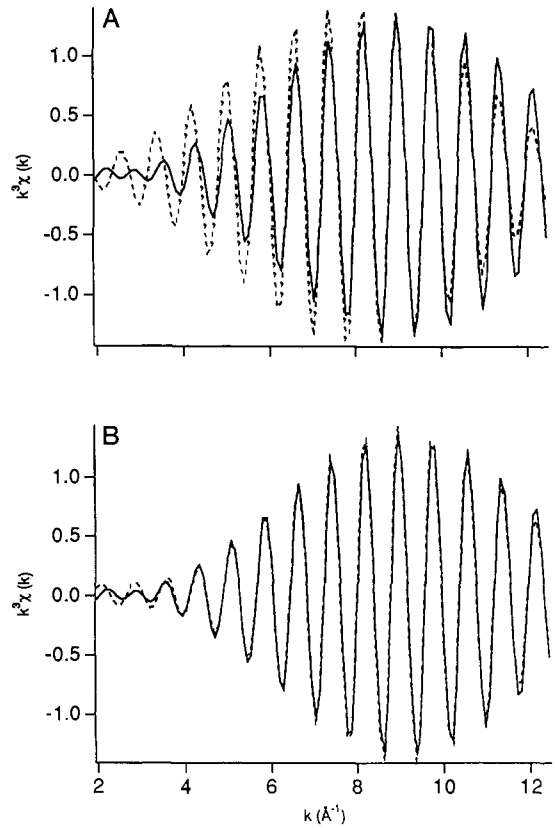

Figure 3. Fourier-filtered EXAFS spectrum arising from atoms in the second coordination sphere (backtransform window = 3.6–4.4 Å) of Ni in *T. roseopersicina* hydrogenase (solid lines). The fits shown (dashed lines) are from Table III. (A) The fit is for a single shell of (2) Fe atoms at a distance of 4.3 Å. (B) The fit is for (2) Ni–Fe = 4.3 Å and (2) Ni–S = 4.2 Å.

from lower Z atoms. Second, most of the EXAFS data analyzed to date have been obtained from "as isolated" or oxidized samples.[20,21] In the case of Fe,Ni H_2ases, two distinct EPR signals are often observed in samples isolated in air, presumably corresponding to two distinct Ni sites. Analysis of this EXAFS data can only yield an average environment that might have significant disorder in the data arising from low Z scatterers.

EXAFS data obtained from an "as isolated" sample of H_2ase from *Desulfovibrio baculatus*[22] suggest that the differences between the first shell data presented here (O,N scatterers are detected) and that previously reported for other Fe,Ni H_2ases (no O,N scatterers detected) may arise from a mixture of Ni sites in the "as isolated" samples used in the earlier studies. The H_2ase from *D. baculatus* is an Fe,Ni,Se enzyme that is isolated in air in a largely EPR silent and active form that lies between forms B and C in the redox sequence involving the Ni site (EPR signals observed for "as isolated" samples account for ca. 10% of the Ni present).[3,18b] Therefore, this sample has ca. 90% of the Ni in a single form. Evidence for 3–4 N,O scattering atoms at the same distance as found for *T. roseopersicina* H_2ase is found from fits of the data from the first coordination sphere of the Ni in the *D. baculatus* case.[22] In fact, the Ni K-edge data, Fourier-filtered first coordination sphere Ni EXAFS, and unfiltered data from the *D. baculatus* H_2ase bear a striking resemblance to the corresponding data from *T. roseopersicina* H_2ase.

Second and Third Coordination Spheres. Although the data from the ca. 0.3 mM sample are noisy, two features from scattering atoms in the second and third coordination sphere of the Ni center in the enzyme rise above the average noise level (Figure 1).[53] The Fourier-transformed spectrum of H_2ase form C reveals a peak at about 4 Å that can be fit with a combination of Fe and S scattering atoms as shown in Table III and Figure 3. The Fourier-filtered spectrum (Figure 3) is fit to an appreciable extent by Fe scattering atoms alone, particularly at high values of k. However, all of the Fe in the protein is believed to be present in Fe,S clusters, and inclusion of S atoms that refine to about the same distance as the Ni–Fe vector substantially improves the fit. The effect of the S-scattering atoms is to model interference that decreases the amplitude of the EXAFS spectrum at low values of k. The best fits are obtained for 2–3 Fe atoms at a distance of 4.3 Å with 1–2 S atoms at 4.2 Å.

The Ni–Fe distance determined is not consistent with incorporation of Ni into an Fe,S core and instead supports a Ni site that is near an Fe_4S_4 cluster. Such a structure is also consistent with the absence of Ni–Fe vectors at ca. 2.6–2.7 Å, a distance that is typical of any Fe,S cluster composed of Fe_2S_2 rhombs[54,55] including the heteronuclear Mo,Fe and V,Fe clusters found in nitrogenases.[56]

The fact that the cluster is observed at all implies the existence of a bridging ligand, since in the absence of such a bridge large Debye–Waller parameters would be expected to render the cluster unobservable. Given the presence of S-donor ligands and the propensity of these ligands to form bridges,[31] it is likely that the site contains either a μ-sulfido or cysteine thiolato bridge. This result is consistent with low-temperature EPR spectra of form C.[18,19] These spectra are complex and show a number of features that have been interpreted as arising from a magnetic interaction between the paramagnetic Ni site and a reduced Fe_4S_4 cluster.

Fits of M–M vectors in the second coordination sphere are complicated by the presence of a large number of possible scattering atoms that could occur at these distances and by multiple scattering effects. A study of oxo-bridged dinuclear Fe complexes has revealed that multiple scattering through the bridging atom does not become severe until the bridging angle exceeds 150°.[57] The same result has been obtained from a limited study of dinuclear Ni complexes. These results are summarized in Table IV. The dimeric complexes $[Ni(SS_2)]_2$ and $[Ni(NS_2SMe)]_2$ can each be described as consisting of two planar complexes joined along an edge by a pair of bridging thiolate ligands. Each complex has a terminal thiolate ligand and either a thioether (SS_2) or a tertiary N-donor in the remaining positions.[31–41] The dimers are bent along the shared edge, giving rise to rather short Ni–Ni distances (2.6–2.7 Å) and very acute Ni–S–Ni bridging angles (77 and 74°, respectively). In the case of $[Ni(NS_2SMe)]_2$, the Ni–Ni distance is determined by EXAFS within ca. 0.03 Å. An accurate Ni–Ni distance is also obtained for $[Ni_2(bimp)(OAc)_2]ClO_4$, although only when scattering arising from C atoms at about the same distance is accounted for.[26] For $\{[Ni(p_3)]_2S\}(BPh_4)_2$, which has an essentially linear Ni–S–Ni bridge, the distance determined is too short by 0.13 Å. The error can be attributed to the combined effects of multiple scattering and transferability problems. In any event, the Ni–Fe distances reported are accurate to 0.1 Å and cannot accommodate incorporation of Ni into an Fe,S cluster, which should exhibit multiple Ni–Fe vectors at 2.6–2.7 Å.[55]

Another interesting feature of Ni–Ni vectors is their varying sensitivity to thermal effects. The planar dimers (e.g. [Ni-

(53) The average noise (1.5) in the Fourier-transformed data was determined by averaging the FT magnitude between r = 2.5–3.6 and 4.3–5.3 Å. The peaks in the Fourier-transformed data near 4 and 6 Å are each 2.3 times the average noise.

(54) (a) Que, L.; Bobrick, M. A.; Ibers, J. A.; Holm, R. H. *J. Am. Chem. Soc.* **1974**, *96*, 4168. (b) Kanatzidis, M. G.; Hagen, W. R.; Dunham, W. R.; Lester, R. K.; Coucouvanis, D. *J. Am. Chem. Soc.* **1985**, *107*, 953. (c) Reynolds, M. S.; Holm, R. H. *Inorg. Chem.* **1988**, *27*, 4494.
(55) Ciurli, S.; Yu, S.-b.; Holm, R. H. *J. Am. Chem. Soc.* **1990**, *112*, 8169.
(56) (a) Conradson, S. D.; Burgess, B. K.; Newton, W. E.; Mortenson, L. E.; Hodgson, K. O. *J. Am. Chem. Soc.* **1987**, *109*, 7507. (b) Flank, A. M.; Weininger, M.; Mortenson, L. E.; Cramer, S. P. *J. Am. Chem. Soc.* **1986**, *108*, 1049. (c) George, G. N.; Coyle, C. L.; Hales, B. J.; Cramer, S. P. *J. Am. Chem. Soc.* **1988**, *110*, 4057.
(57) (a) Co, M. S.; Hendrickson, W. A.; Hodgson, K. O.; Doniach, S. *J. Am. Chem. Soc.* **1983**, *105*, 1144. (b) Teo, B. K. *J. Am. Chem. Soc.* **1981**, *103*, 3990.

Table III. Fits from Second and Third Coordination Sphere Fourier-Filtered Ni EXAFS Data from Hydrogenase[a]

	backtransform window, Å	*N*	*r*, Å	$10^3\Delta\sigma^2$, Å^2	correl coeff > 0.6	*R*
2nd coordination sphere	3.6–4.4	1	Ni–Fe = 4.302 (1)	−5.0 (1)		0.09
		2	Ni–Fe = 4.301 (2)	−0.7 (2)		0.21
		3	Ni–Fe = 4.300 (3)	2.4 (3)		0.32
		4	Ni–Fe = 4.299 (4)	5.2 (5)		0.39
		1	Ni–S = 4.443 (2)	−6.6 (2)		0.21
		2	Ni–S = 4.448 (2)	−2.7 (3)		0.27
		3	Ni–S = 4.452 (3)	0.3 (4)		0.37
		4	Ni–S = 4.455 (4)	3.2 (6)		0.45
		1 1	Ni–Fe = 4.304 (1) Ni–S = 4.310 (4)	−5.2 (1) 13.3 (7)		0.03
		1 2	Ni–Fe = 4.303 (1) Ni–S = 4.296 (3)	−5.1 (1) 26 (6)		0.02
		2 1	Ni–Fe = 4.279 (1) Ni–S = 4.204 (2)	−2.3 (1) −3.3 (1)	$r_S/r_{Fe} = 0.84$; $r_S/\sigma^2_{Fe} = -0.86$; $r_{Fe}/\sigma^2_S = 0.74$	0.03
		2 2	Ni–Fe = 4.297 (5) Ni–S = 4.240 (2)	−2.2 (1) 6.0 (3)	$r_S/r_{Fe} = 0.77$; $\sigma^2_S/\sigma^2_{Fe} = 0.80$	0.04
		2 3	Ni–Fe = 4.299 (6) Ni–S = 4.237 (3)	−1.8 (7) 13.1 (5)	$r_S/r_{Fe} = 0.65$; $\sigma^2_S/\sigma^2_{Fe} = 0.68$	0.06
		3 1	Ni–Fe = 4.256 (1) Ni–S = 4.163 (1)	2.6 (1) −5.3 (6)	$r_S/\sigma^2_{Fe} = -0.90$; $r_{Fe}/\sigma^2_S = 0.73$	0.04
		3 2	Ni–Fe = 4.271 (1) Ni–S = 4.194 (2)	−0.1 (1) −0.8 (1)	$r_S/r_{Fe} = 0.84$; $r_S/\sigma^2_{Fe} = -0.81$; $r_{Fe}/\sigma^2_S = 0.71$	0.04
		3 3	Ni–Fe = 4.288 (1) Ni–S = 4.218 (3)	−0.2 (1) 4.9 (3)	$r_S/r_{Fe} = 0.79$; $r_{Fe}/\sigma^2_S = 0.62$; $\sigma^2_S/\sigma^2_{Fe} = 0.69$	0.07
3rd coordination sphere	5.5–6.5	2	Ni–Fe = 6.230 (2)	−5.3 (2)		0.22
		2 2	Ni–Fe = 6.234 (2) Ni–S = 6.248 (2)	−5.6 (2) 6.7 (3)	$r_S/r_{Fe} = 0.62$; $r_{Fe}/\sigma^2_S = -0.69$; $\sigma^2_S/\sigma^2_{Fe} = 0.67$	0.17
2nd + 3rd coordination spheres	3.6–6.5	2 2 2 2	Ni–Fe = 4.278 (9) Ni–S = 4.213 (2) Ni–Fe = 6.226 (5) Ni–S = 6.21 (3)	−3.7 (6) −0.3 (2) −6.4 (5) 3 (4)	no correlations between 2nd and 3rd coordination sphere parameters	0.45
1st + 2nd + 3rd coordination spheres	1.1–6.5	2 3	Ni–S = 2.215 (8) Ni–N = 2.053 (9)	0.5 (9) −4.8 (8)	$r_S/r_N = -0.77$; $\sigma^2_N/\sigma^2_S = -0.62$	1.30
		2 3 2	Ni–S = 2.214 (7) Ni–N = 2.054 (8) Ni–Fe = 4.301 (8)	0.6 (8) −4.9 (7) −1.6 (8)	$r_S/r_N = -0.77$; $\sigma^2_N/\sigma^2_S = -0.65$	1.12
		2 3 2 2	Ni–S = 2.213 (7) Ni–N = 2.055 (7) Ni–Fe = 4.295 (14) Ni–S = 4.25 (4)	0.7 (8) −5.0 (7) −4 (1) 0 (5)	$r_S/r_N = -0.78$; $r_{Fe}/r_{S(2nd\ shell)} = 0.88$; $\sigma^2_{Fe}/\sigma^2_{S(2nd\ shell)} = 0.89$	1.08
		2 3 2 2 2	Ni–S = 2.214 (7) Ni–N = 2.054 (6) Ni–Fe = 4.290 (12) Ni–S = 4.242 (28) Ni–Fe = 6.225 (6)	0.6 (6) −4.9 (5) −4 (1) 1 (3) −5.6 (6)	$r_S/r_N = -0.77$; $\sigma^2_S/\sigma^2_N = -0.65$ $r_{Fe}/r_{S(2nd\ shell)} = 0.86$; $\sigma^2_{Fe}/\sigma^2_{S(2nd\ shell)} = 0.89$	0.84
		2 3 2 2 2	Ni–S = 2.214 (6) Ni–N = 2.054 (6) Ni–Fe = 4.289 (12) Ni–S = 4.240 (27) Ni–Fe = 6.225 (9) Ni–S = 6.20 (6)	0.6 (6) −4.9 (5) −4 (1) 1 (3) −6 (6) 6 (8)	$r_S/r_N = -0.77$; $\sigma^2_S/\sigma^2_N = -0.65$ $\sigma^2_{Fe(2nd\ shell)}/\sigma^2_{S(2nd\ shell)} = 0.83$; $r_{Fe(3rd\ shell)}/r_{S(3rd\ shell)} = 0.79$; $\sigma^2_{Fe(3rd\ shell)}/\sigma^2_{S(3rd\ shell)} = 0.85$	0.82

[a] Parameters are defined in Table I.

$(NS_2SMe)]_2$) exhibit features in the Fourier-transformed spectra attributable to the presence of a Ni–Ni vector (Figure 4). This feature is less apparent in the Fourier-transformed spectrum at room temperature, although fits of data collected at room temperature are substantially improved by including the Ni–Ni vector, and it is refined to an appropriate distance (Table IV). In contrast, in $[Ni_2(bimp)(OAc)_2]ClO_4$ and $\{[Ni(p_3)]_2S\}(BPh_4)_2$ the Ni–Ni vector is easily observed in the room temperature spectrum. This result implies that the Ni scattering is particularly sensitive to motions involving the bridging linkage. In $[Ni_2(bimp)(OAc)_2]$-ClO_4, the dinuclear center is triply bridged and presumably fairly rigidly held at a Ni–O–Ni bridging angle of 116.7 (5)°.[58] A linear bridge is found in $\{[Ni(p_3)]_2S\}(BPh_4)_2$,[59] while the other two dimers involve edge-sharing in the fashion of a hinge. Apparently, the motions allowed by the hinge give rise to motions reflected in temperature-dependent Debye–Waller parameters.

(58) Buchanan, R. M.; Mashuta, M. S.; Oberhauser, K. J.; Richardson, J. F. *J. Am. Chem. Soc.* **1989**, *111*, 4497.
(59) Mealli, C.; Midollini, S.; Sacconi, L. *Chem. Commun.* **1975**, 765.

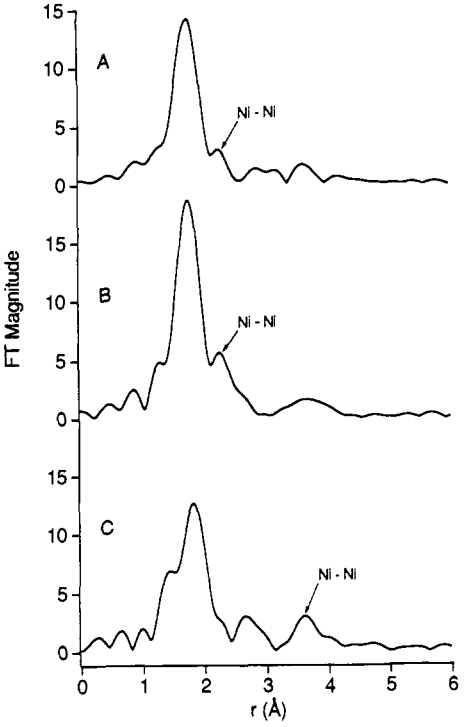

Figure 4. Fourier-transformed EXAFS spectra from dinuclear Ni complexes: (A) $[Ni(NS_2SMe)]_2$ at room temperature; (B) $[Ni(NS_2SMe)]_2$ at 77 K; (C) $\{[Ni(p_3)]_2S\}(BPh_4)_2$ at room temperature.

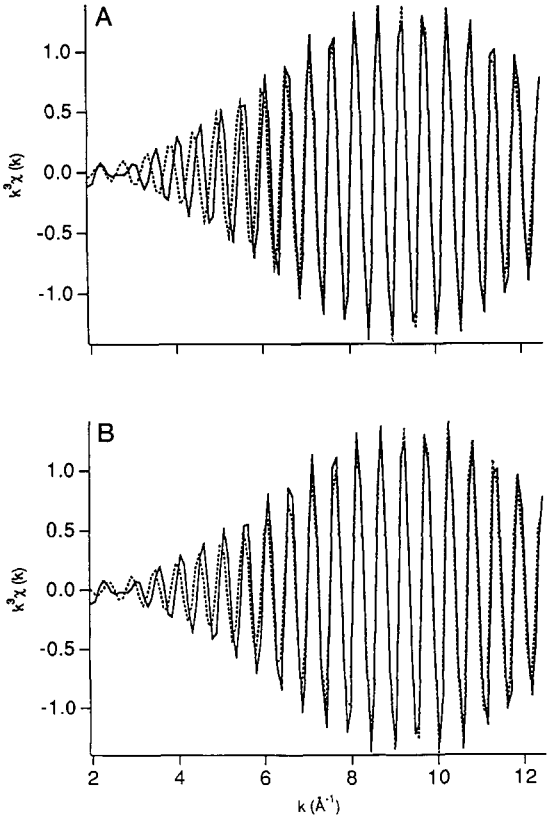

Figure 5. Fourier-filtered EXAFS spectrum arising from atoms in the third coordination sphere (backtransform window = 5.5–6.5 Å) of Ni in *T. roseopersicina* hydrogenase (solid lines). The fits shown (dashed lines) are from Table III. (A) The fit is for a single shell of (2) Fe atoms at a distance of 6.2 Å. (B) The fit is for (2) Ni–Fe = 6.2 Å and (2) Ni–S = 6.2 Å.

Peaks at ca. 4 Å in Fourier-transformed spectra can arise from the presence of third coordination sphere C and N atoms of histidine imidazole ligands.[60] However, several facts argue against this assignment in this case: (1) The distance found is longer than typically observed for histidine imidazole atoms and the Fourier-filtered EXAFS arising from atoms at 4 Å cannot be even approximately fit by a single shell of C atoms (particularly involving a maximum of one possible histidine ligand, vide infra). (2) Scattering from histidine ligands is generally accompanied by the observation of a peak due to scattering by second coordination sphere C atoms at about 3 Å as well as atoms in the third coordination sphere. This peak is usually (but not always) of similar or greater intensity than the third coordination sphere peak. Examination of the hydrogenase data (Figure 1) reveals little evidence of any scattering from atoms in this range. (3) There is only equivocal evidence indicating the involvement of a single histidine ligand in the Ni coordination sphere. ESEEM studies reveal a single weakly coupled N atom that might be assigned to the distal N atom of a histidine ligand. The ESEEM data could also arise from a nearby N atom that is not a metal ligand. (4) The existence of a novel Ni,Fe,S cluster is supported by EPR data that are consistent with magnetic interactions between a Ni site and an Fe,S cluster. (5) The magnitude of the M–M vector near 4 Å in the Fourier-transformed spectrum (Figure 1) is comparable with that shown for $\{[Ni(p_3)]_2S\}(BPh_4)_2$ in Figure 4C and involves a similar distance. (6) The presence of Fe scattering atoms in the second coordination sphere of Ni arising from a nearby Fe,S

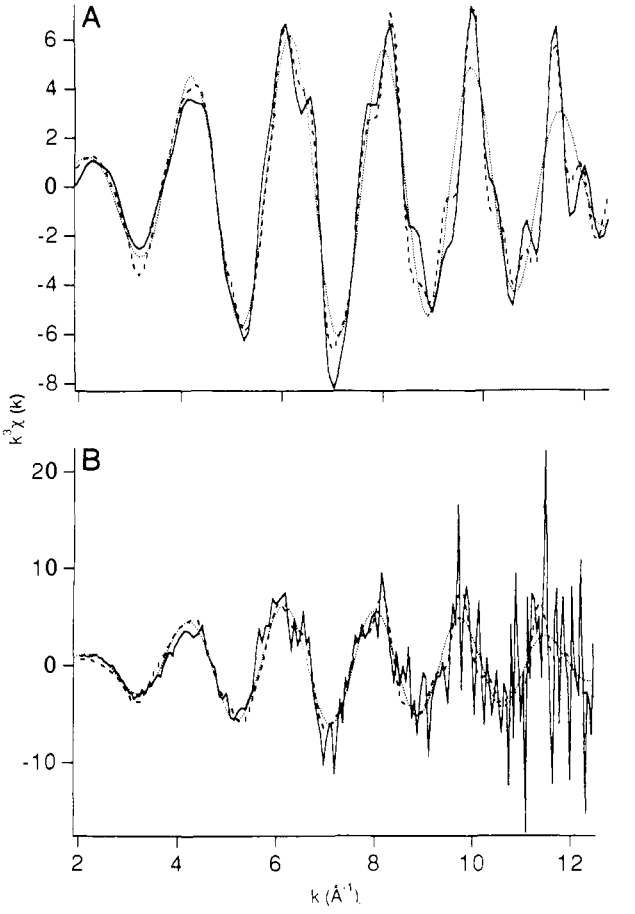

Figure 6. Multishell fits to EXAFS data arising from the Ni sites in *T. roseopersicina* hydrogenase (solid lines). (A) Fourier-filtered spectrum (backtransform window = 1.1–6.5 Å) (solid line), first coordination sphere fit from Figure 2 (dotted line), and multishell fit including second and third shell Fe and S scattering atoms (dashed line). The multishell fit shown is from Table III and is the same as shown in Figure 1. (B) k^3-weighted unfiltered EXAFS data (solid line), first coordination sphere fit from Figure 2 (dotted line), and a multishell fit (dashed line) from Table V consisting of (3) Ni–N = 2.06 Å, (2) Ni–S = 2.21 Å, (2) Ni–Fe = 4.3 Å, (2) Ni–S = 4.3 Å, (2) Ni–Fe = 6.2 Å, and (2) Ni–S = 6.2 Å.

(60) (a) Strange, R. W.; Blackburn, N. J.; Knowles, P. F.; Hasnain, S. S. *J. Am. Chem. Soc.* **1987**, *109*, 7157. (b) Co, M. S.; Scott, R. A.; Hodgson, K. O. *J. Am. Chem. Soc.* **1981**, *103*, 986.

Table IV. Analysis of Dimeric Ni Complexes for Second Coordination Sphere Ni–Ni Vectors[a]

compounds	backtransform window, Å	N	r, Å	$10^3\Delta\sigma^2$, Å^2	R	crystallographic Ni–Ni distance, Å	ref
$[Ni(SS_2)]_2$ (77 K)	1.1–2.7	1	Ni–Ni = 2.729 (4)	−0.6 (5)	0.62	2.733 (5)	41
		4	Ni–S = 2.169 (1)	−0.4 (1)			
$[Ni(NS_2SMe)]_2$ (77 K)	1.1–2.7	1	Ni–Ni = 2.657 (3)	2.0 (6)	0.23		
		3	Ni–S = 2.168 (1)	−1.6 (5)			
		1	Ni–N = 1.854 (4)	−0.7 (6)			
$[Ni(NS_2SMe)]_2$	1.1–2.7	1	Ni–Ni = 2.695 (5)	6.7 (9)	0.27	2.635 (1)	31
		3	Ni–S = 2.164 (1)	0			
$[Ni_2(bimp)(OAc)_2]ClO_4$	2.0–3.6	1	Ni–Ni = 3.412 (8)	2.9 (9)	0.37	3.422 (4)	55
		1.7 (3)	Ni–C = 3.660 (20)	not refined			
		11.0 (5)	Ni–C = 2.916 (4)	not refined			
$[(Ni(p_3))_2S](BPh_4)_2$	3.1–4.1	1	Ni–Ni = 3.943 (1)	−2.4 (1)	0.11	4.068 (4)	56

[a] Parameters are defined in Table I.

Table V. Fits of Unfiltered Ni EXAFS Data from Hydrogenase[a]

N	r, Å	$10^3\Delta\sigma^2$, Å^2	correl coeff > 0.6	R
5	Ni–N = 2.060 (6)	−5.9 (7)		4.10
1	Ni–S = 2.217 (23)	−4 (3)	r_N/σ^2_S = 0.63	3.95
4	Ni–N = 2.042 (21)	−3 (2)	r_S/r_N = −0.71; r_S/σ^2_N = −0.63	
2	Ni–S = 2.204 (23)	1 (3)	r_S/r_N = −0.86; σ^2_S/σ^2_N = −0.89	3.90
3	Ni–N = 2.063 (24)	−5 (3)		
3	Ni–S = 2.212 (17)	3 (3)	r_S/σ^2_N = 0.73; σ^2_S/σ^2_N = −0.76	3.89
2	Ni–N = 2.063 (14)	−8 (2)		
4	Ni–S = 2.222 (13)	6 (2)		3.89
1	Ni–N = 2.060 (12)	−12 (1)		
5	Ni–S = 2.214 (6)	3 (1)		4.10
2	Ni–S = 2.207 (21)	0 (3)	r_S/r_N = −0.86; σ^2_N/σ^2_S = −0.89	3.85
3	Ni–N = 2.059 (26)	−4 (3)		
2	Ni–Fe = 4.303 (18)	−2 (2)		
2	Ni–S = 2.209 (22)	0 (3)	r_S/r_N = −0.84; σ^2_S/σ^2_N = −0.82;	3.84
3	Ni–N = 2.056 (25)	−4 (3)	$\sigma^2_{Fe}/\sigma^2_{S(2nd\ shell)}$ = 0.98	
2	Ni–Fe = 4.30 (4)	−5.5 (5)		
2	Ni–S = 4.27 (9)	−2 (1)		
2	Ni–S = 2.208 (22)	0 (3)	r_S/r_N = −0.84;	3.78
3	Ni–N = 2.058 (25)	−4 (3)	σ^2_S/σ^2_N = −0.84;	
2	Ni–Fe = 4.30 (4)	−4 (1)	$\sigma^2_{Fe}/\sigma^2_{S(2nd\ shell)}$ = 0.96	
2	Ni–S = 4.27 (10)	1 (3)		
2	Ni–Fe = 6.223 (22)	−5.6 (6)		
2	Ni–S = 2.208 (22)	0 (3)	r_S/r_N = −0.84;	3.78
3	Ni–N = 2.058 (6)	−4 (3)	σ^2_S/σ^2_N = −0.84;	
2	Ni–Fe = 4.30 (4)	−2 (5)	$\sigma^2_{Fe(2nd\ shell)}/\sigma^2_{S(2nd\ shell)}$ = 0.96	
2	Ni–S = 4.27 (10)	1 (1)		
2	Ni–Fe = 6.225 (26)	−6 (3)		
2	Ni–S = 6.2 (4)	7 (6)		

[a] Parameters are defined in Table I.

cluster implies the existence of third coordination sphere Fe scattering atoms as well. Inspection of the Fourier-transformed spectrum (Figure 1) reveals a third peak at ca. 6 Å that can be accommodated by this model but not by a model involving an imidazole ligand.

The data in Table III and Figure 5 show that the peak at ca. 6 Å in the Fourier-filtered spectrum can be fit by Fe or a combination of Fe and S scattering atoms at 6.2 Å. In this case, the addition of S scattering atoms has a similar effect as in the second coordination sphere data, although only a marginal improvement in the fit is obtained.

Multiple Shell Fits and Fits Generated to Unfiltered Data. The results of multiple shell fits to Fourier-filtered data in the 1.1–6.5-Å range are summarized in Table III and Figure 6. As expected, these fits reveal that the total EXAFS spectrum is dominated by scattering atoms in the first coordination sphere, which remains essentially unchanged from that obtained from Fourier filtering the first shell data. However, the addition of the Fe scattering atoms in the second and third coordination spheres significantly improves the fits. The S scattering atoms at $r > 4$ Å make a negligible contribution to the overall EXAFS spectrum (Table III). This would be expected because of the smaller back-scattering cross section of the S atoms and the distances involved.

Fits generated with unfiltered data do not suffer from truncation effects and therefore generally give the most accurate bond lengths. These fits are summarized in Table V and Figure 6 and do not differ substantially from those obtained with Fourier-filtered data. Assuming a five-coordinate geometry, the best fits were obtained for 3 ± 1 S-donor atoms at 2.21 (2) Å and 2 ± 1 N-donor atoms at 2.06 (2) Å. Again, the addition of 2 ± 1 Fe scattering atoms in the second and third coordination spheres improves the fits obtained, but the outer-sphere S atoms make an insignificant contribution to the EXAFS spectrum. The Ni–Fe distances obtained, 4.3 (1) and 6.2 (1) Å, are unchanged from those obtained with Fourier-filtered data.

In both multishell fits, a number of correlations between parameters for scattering atoms in the same coordination sphere exist. This is expected when the absorber–scatterer distances are within ca. 0.2 Å. There are no correlations between parameters for scattering atoms in different coordination spheres or with the

baseline in the case of fits to unfiltered data where the baseline can also be refined.

Conclusions

Information regarding the structure of the Ni site in *Thiocapsa roseopersicina* hydrogenase poised in form C has been obtained from the analysis of features in the Ni K-edge EXAFS spectrum and is supported by data from structurally characterized model compounds and the analysis of X-ray absorption edge structure. The Ni ligands include 2 ± 1 S,Cl donors at 2.21 (2) Å and 3 ± 1 N,O donors at 2.06 (2) Å. Features arising from scattering atoms in the second and third coordination sphere can be accommodated by a model involving the association of the Ni center with an Fe_4S_4 cluster. The second coordination sphere Ni-Fe distance (4.3 Å) is too large for the Ni to be incorporated into an Fe,S cluster, and the absence of a 2.6-2.7 Å Ni-Fe vector suggests that a novel Ni,Fe,S cluster exists in Ni,Fe H_2ases. The observation of scattering from the Fe,S cluster implies the existence of a ligand that bridges between the cluster and the Ni site. The involvement of the Fe,S cluster is further corroborated by the observation of features that can be fit by Fe atoms in the third coordination sphere at a distance of 6.2 Å.

The structure that emerges from the EXAFS analysis has several features reminiscent of the structure of the metal cluster in *E. coli* sulfite reductase.[61] This enzyme contains a siroheme Fe atom linked to an Fe_4S_4 cluster via an Fe-S-Fe bridge. The closest Fe_{heme}-$Fe_{cluster}$ distance is 4.4 Å, with an average Fe_{heme}-$Fe_{cluster}$ distance of 4.7 Å. The closest S atom in the cluster lies at 4.3 Å. The distal Fe atoms in the cluster lie at 6.4 and 6.7 Å. Assuming a similar linkage involving a sulfido or thiolato bridge between the Ni center and an Fe_4S_4 cluster, several structures involving one or two Fe_4S_4 clusters can be envisioned that accommodate the Ni-Fe,S distances found in the second and third coordination spheres of the Ni. These results are not inconsistent with speculation that the H cluster[15] associated with H_2 activation in Fe-only hydrogenases may have a similar structure to the Ni,Fe,S cluster in Fe,Ni,S H_2ases, where a nonheme Fe is substituted for the Ni atom.[62]

Acknowledgment. This work was supported by NIH Grant GM-38829 (M.J.M.)) and a travel grant from the Faculty-Student Research Support Program at the National Synchrotron Light Source. Acknowledgement is also made to the donors of the Petroleum Research Fund administered by the American Chemical Society (P.K.M.). We thank Dr. Stephen P. Cramer for the use of his 13-element Ge X-ray fluorescence detector, Dr. John F. Stoltz, Joyce P. Whitehead, and Denise L. Driscoll for assistance in culturing *T. roseopersicina* and in the purification of hydrogenase from this source. We are indebted to Dr. I. N. Gogotov for the gift of the original bacterial culture, to Prof. Robert Buchanan for the gift of $[Ni(bimp)(OAc)_2]ClO_4$, to the National Biostructures Participating Research Team administration for beam time allocations, and to Dr. Syed Khalid, Dr. Anne True, Prof. Robert Scarrow, and Prof. Lawrence Que, Jr., for experimental support.

Supplementary Material Available: Table of fits generated to Fourier-filtered EXAFS spectra from 18 model compounds (24 pages). Ordering information is given on any current masthead page.

(61) McRee, D. E.; Richardson, D. C.; Richardson, J. S.; Siegel, L. M. *J. Biol. Chem.* **1986**, *261*, 10277.

(62) Adams, M. W. W.; Johnson, M. K.; Zambrano, I. C.; Mortenson, L. E. *Biochimie* **1986**, *68*, 35.

Synthesis of Deoxydinucleoside Phosphorodithioates[1]

Wolfgang K.-D. Brill,[†] John Nielsen,[‡] and Marvin H. Caruthers*

Contribution from the Department of Chemistry and Biochemistry, Campus Box 215, University of Colorado, Boulder, Colorado 80309-0215. *Received September 28, 1990*

Abstract: The synthesis of a new class of DNA analogues called phosphorodithioate DNA is described. This analogue, which has a deoxynucleoside-OPS_2O-deoxynucleoside internucleotide linkage, is isosteric and isopolar with the normal phosphodiester, inert toward nucleases, and potentially useful for a large number of biochemical and biological applications. Two methods are described for synthesizing this derivative. One route begins by condensing a deoxynucleoside phosphorodiamidite with a second appropriately protected deoxynucleoside to yield a deoxydinucleoside phosphoramidite. Sulfhydrolysis with H_2S generates the H-phosphonothioate, which upon oxidation with sulfur yields the deoxydinucleoside phosphorodithioate. Alternatively, sequential treatment of the deoxydinucleoside phosphoramidite with a mercaptan and sulfur yields the deoxydinucleoside phosphorodithioate triester. These deoxydinucleotides in protected form can then be used to introduce the dithioate internucleotide linkage into DNA. The second route for generating dithioate DNA uses deoxynucleoside phosphorothioamidites. Two derivatives, the deoxynucleoside 3'-*N*,*N*-dimethyl- or 3'-(*N*,*N*-tetramethylenephosphorothioamidite), were found to be especially attractive synthons as they could be prepared in stable form via a one-flask synthesis procedure and used to form the deoxydinucleoside thiophosphite rapidly (1-2 min with tetrazole as activator) in high yield. Subsequent oxidation with sulfur generates the completely protected phosphorodithioate linkage.

During the past decade, polynucleotides modified at phosphorus have found many new and potentially important applications in biochemistry and molecular biology. These include their use for studying enzyme mechanisms,[2] the interaction of proteins with nucleic acids,[3] and potentially as therapeutic drugs.[4] Although a large number of analogues have been synthesized and tested for biochemical reactivity, only a few are currently of interest. These include the polynucleotide methylphosphonates,[5] phos-

[†] Department of Organic Chemistry, Johannes Gutenberg Universität, Postfach 3980, J. J. BecherWeg 18-20, D-6500 Mainz, Germany.
[‡] Present address: Harboe's Laboratorium, Guldborgvej 22, DK-2000 Frederiksberg F, Denmark.

(1) Part 33 in a series on nucleotide chemistry. Part 32: Caruthers, M. H.; Beaton, G.; Cummins, L.; Dellinger, D.; Graff, D.; Ma, Y.-X.; Marshall, W. S.; Sasmor, H.; Shankland, P.; Wu, J. V.; Yau, E. K. *Nucleosides Nucleotides*, in press. This research was supported by the National Institutes of Health (Grant GM25680). Abbreviations: DMT, 4,4'-dimethoxytrityl; DMTOH, 4,4'-dimethoxytritanol; B, thymine, 4-*N*-benzoylcytosine, 6-*N*-benzoyladenine, 2-*N*-isobutyrylguanine.

(2) Connolly, B. A.; Potter, B. V. L.; Eckstein, F.; Pingoud, A.; Grotjahn, L. *Biochemistry* **1984**, *23*, 3443.

0002-7863/91/1513-3972$02.50/0